JTTEE5 7:484-488

Effects of Power Level on Characteristics of Vacuum Plasma Sprayed Hydroxyapatite Coating

C. Chang, J. Shi, J. Huang, Z. Hu, and C. Ding*

(Submitted 13 October 1997; in revised form 20 April 1998)

In this study, hydroxyapatite coatings were obtained with a vacuum plasma spray system at different power levels that were achieved by altering the plasma current and voltage. The effects of spray power level on coating characteristics were investigated. X-ray diffraction was used to identify the crystallinities of as-sprayed coatings, Electron Probe Microanalysis was employed to detect the surface chemical composition of as-sprayed coatings and Scanning Electron Microscopy revealed the microstructure. The results indicated that spray power greatly affected the crystallinity, chemical composition, and microstructure of as-sprayed hydroxyapatite coatings, which were linked to the melting state of hydroxyapatite powder.

Keywords amorphorization, crystallinity, hydroxyapatite coating, microstructure, vacuum plasma spraying

1. Introduction

Hydroxyapatite is biocompatible and has been used as biomaterial for numerous medical applications, such as orthopedic and dental implants (Ref 1-2). It has favorable osteoconductive and bioactive properties that could promote rapid bone formation and strong biological fixation to bony tissues (Ref 3-4). This material has similar chemical composition and crystal structure to apatite in the human skeletal system and, therefore, is suitable for bone substitution and reconstruction. However, the poor mechanical properties restrict its use in load bearing areas (Ref 5-7). Recent developments include the application of advanced surface technology to create new ways of incorporating hydroxyapatite with mechanically strong metallic materials to enhance osseointegration.

Methods used to deposit hydroxyapatite onto metallic substrates include sol-gel methods, chemical deposition, ion-sputtering deposition, thermal spraying, etc. (Ref 8-11). Among these, plasma spraying has proven to be the most preferred choice and since 1985, implants with plasma sprayed hydroxyapatite coatings have been used in clinical practice (Ref 12).

In this study, hydroxyapatite coatings were manufactured using a vacuum plasma spray system. X-ray diffraction and scanning electron microscopy were used to investigate the effect of plasma spray power on the characteristics of as-sprayed coatings.

C. Chang, J. Shi, J. Huang, Z. Hu, and **C. Ding,** Shanghai Institute of Ceramics, Chinese Academy of Sciences, 1295 Dingxi Rd, Shanghai, 200050, Republic of China. Contact e-mail: ckchang@mail1.sjtu.edu.cn

*Presently at School of Materials Science and Engineering, Shanghai Jiaotong University, 1954 Huashan Road, Shanghai 200030, Republic of China.

2. Experimental Procedures

Vacuum plasma spraying (VPS) was carried out with a VPS system from Sulzer Metco, Switzerland, under the general con-

Table 1 Vacuum plasma spray parameters

Plasma spraying parameters	Value
Primary spray gas	Ar, 50 slpm
Secondary plasma gas	H_2, 10 slpm
Carrier gas	Ar, 1.5 slpm
Powder flow rate, g/min	20
Plasma jet type	F4-VB
Injector, mm	ϕ 1.8
Chamber pressure, mbar	150
Spray power, kW	30-45
Spray distance, mm	275
Thickness of coating controlled, μm	100

Fig. 1 Morphology of starting powder

ditions listed in Table 1. The substrates, Ti6Al4V alloy, were of 20 by 10 by 4 mm dimensions, sandblasted with alumina grit to an average surface roughness of 20 μm, and cleaned in ethyl alcohol. The starting powder, hydroxyapatite, was supplied by Sulzer Metco, with a size distribution of 1 - 180 μm and a mean size of 100 μm. Figure 1 shows the scanning electron micrograph (SEM) of the starting powder, indicating that the powder was chemically synthesized and mechanically crushed into small irregularly shaped particles. Chemical analysis supplied by the manufacturer indicated that the powder was of high purity, with impurities of: As (<0.5 μg/g), Cd (<0.2 μg/g), Hg (<0.5 μg/g), and Pb (<1μg/g). An x-ray diffraction (XRD) scan of the as-received powder, (Fig. 2) when compared with JCPDS standard (9-0432), indicates that only well crystallized hydroxyapatite is present in the powder as seen from the sharp peaks and flat baselines. No other phases were detected.

The experimental design employed for hydroxyapatite is shown in Table 2. Changes in the spray current and voltage investigated the influence of spray power on the characteristics of the as-sprayed coatings.

Phase analysis of as-sprayed coatings was conducted using an XRD at 40 keV and 70 mA and using 1.5418 A copper Kα radiation on wavelength. Scans were run from 20 to 60 °, with a 2θ step of 0.02 ° and a time increment of 3 s. Phase composition was determined according to JCPDS standards.

The crystallinities of as-sprayed coatings were calculated from the XRD patterns using the peak intensities of the (211), (112), and (300) planes of hydroxyapatite. Standard curves for calculating crystallinity were made from XRD patterns of samples with hydroxyapatite contents of 10, 30, 50, 70, and 90 wt% from a mixture of hydroxyapatite powder and an amorphous $CaO\text{-}SiO_2\text{-}P_2O_5$ bioglass. The peak intensities of all three lattice planes were plotted against hydroxyapatite content, and a linear relationship was discovered (Fig. 3).

Surface morphology was observed by SEM. Samples were sputter coated with a 5 nm thick gold film. The chemical composition of Ca and P on the surface was analyzed by electron probe microanalysis (EPMA) using Ca and P Kα rays, respectively.

3. Results and Discussion

3.1 Crystallinity of Hydroxyapatite Coatings

XRD patterns of hydroxyapatite coatings sprayed at different spray power levels are shown in Fig. 4. The patterns indicate that

Table 2 Current and voltage designed for vacuum plasma spraying of hydroxyapatite coatings

Parameter	Experiment						
	1	2	3	4	5	6	7
Current, A	600	600	700	700	700	700	700
Voltage, V	50	55	50	55	58	60	65
Power, kW	30	33	35	8.5	40.6	42	45.5

Table 3 Diffraction intensities and crystallinities of coatings sprayed at different power levels

Spray power level, kW	Diffraction intensity, cps			Crystallinity, %		
	(211)	(112)	(300)	(211)	(112)	(300)
30	2913	1523	1893	95.3	93.4	96.1
33	2037	1027	1295	66.6	63.6	66.1
35	1387	707	846	45.4	44.3	43.6
38.5	986	513	645	32.4	32.7	33.5
40.6	696	327	437	23.0	21.5	23.1
42	427	217	283	14.2	14.8	15.3
45.5	253	97	138	8.5	7.6	8.0

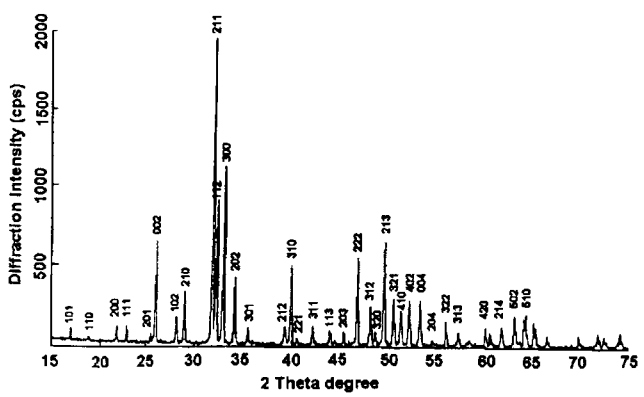

Fig. 2 XRD pattern of starting powder

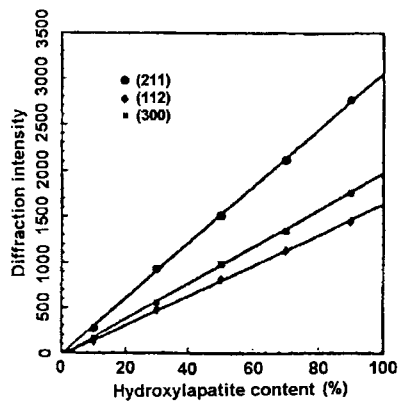

Fig. 3 Standard curve for calculation crystallinity of coating

the coatings matched peak positions with those of the JCPDS file for hydroxyapatite (9-0432). Compared with the pattern of the starting powder, the XRD patterns of as-sprayed coatings show a decrease in peak intensity. It can be concluded that crystallinity of the coating decreases with an increase in plasma spray power level. At power levels of 45.5 kW, the as-sprayed coating mainly consists of amorphous hydroxyapatite indicated by the broad background in the XRD pattern in the 25°-35° 2θ region. Peak intensities of (211), (112), and (300) lattice planes and the calculated crystallinities of coatings sprayed under different power are presented in Table 3.

The relationship between spray power level and coating crystallinity is also shown in Fig 5, which revealed a sharp decrease in crystallinity with an increase of spray power. The formation of the amorphous phase may arise from melting of the hydroxyapatite particles. In the spray process, the particles experience melting and resolidification processes. In the melting process, the starting powder changes from crystalline to an amorphous phase, while in the resolidification process, the amorphous phase begins to recrystallize (Ref 13). Recrystallization rarely occurs (for a 20 μm thick hydroxyapatite coating) (Ref 14) and, thus, the melting process plays a large role in de-

Table 4 EPMA Results of as-sprayed coatings

Spray power, kW	Element molar percentage, %				Oxide weight percentage, %		
	Ca	P	O	Ca/P molar ratio	CaO	P_2O_5	CaO/P_2O_5
Starting powder	24.41	14.62	60.97	1.67	56.83	43.17	1.31
30	25.05	14.26	60.69	1.76	58.08	41.92	1.38
33	25.57	13.96	60.47	1.83	59.1	40.90	1.44
35	25.99	13.72	60.29	1.89	59.98	40.02	1.49
38.5	26.50	13.42	60.06	1.97	60.88	39.12	1.55
40.6	27.20	13.03	59.77	2.08	62.21	37.79	1.64
42	27.97	12.59	59.44	2.22	63.66	36.36	1.75
45.5	28.20	12.46	59.34	2.26	64.1	35.90	1.78

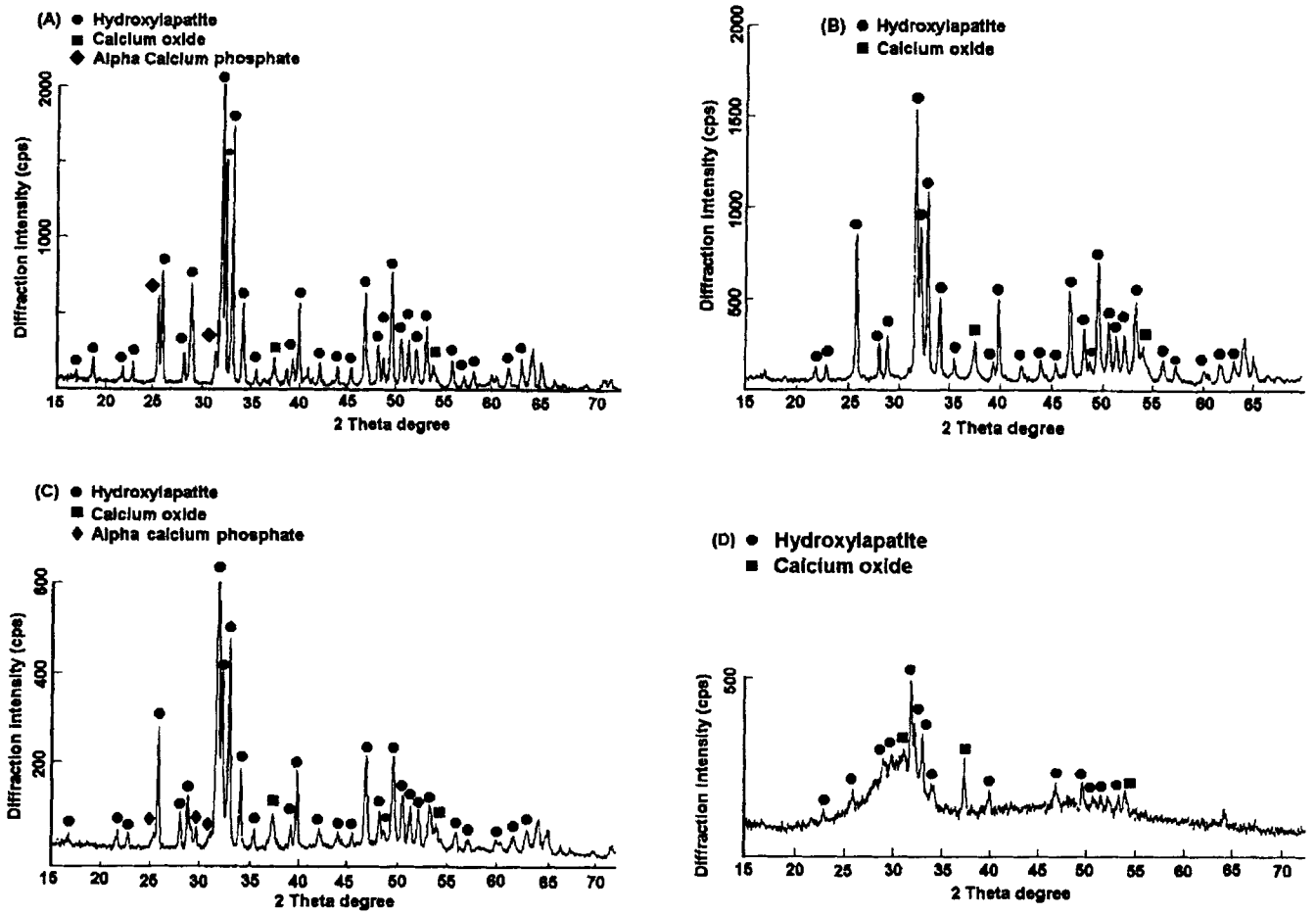

Fig. 4 XRD patterns of as-sprayed coatings. (a) Coating sprayed at 30 kW. (b) Coating sprayed at 35 kW. (c) Coating sprayed at 40.6 kW. (d) Coating sprayed at 45.5 kW

termining the amorphous phase content of the coating. It was apparent that under a higher spray power level the hydroxyapatite powder was molten to a higher degree thus creating coatings with lower crystallinity.

3.2 *Decomposition of Hydroxyapatite during the Plasma Process*

Decomposition of hydroxyapatite occurs during the VPS process as can be confirmed by XRD patterns (Fig 4). Calcium oxide is detected as a new phase with the coating. This suggests a phase change from hydroxyapatite to calcium oxide in the coating process (Ref 15). Chemical analysis made by EPMA is given in Table 4 and the relationship between spray power level and chemical composition is shown in Fig. 6 and 7. It can be seen from the figures that CaO content in the coatings increased with a higher spray power level while P_2O_5 content decreased. The Ca/P molar ratio increased significantly from 1.67 for the starting powder to 2.26 for coatings sprayed under 45.5 kW. These results suggest that the decomposition of hydroxyapatite is promoted by an increase in spray power level.

3.3 *Microstructure of As-Sprayed Hydroxyapatite Coating*

Examination of the surface structure is a means of assessing the coating microstructure (Ref 16). SEM micrographs (Fig. 8), reveal a change in surface morphology of as-sprayed coatings under different spray power levels. Figure 8(a) shows a coating morphology consisting mainly of unmolten particles. Some partially melted particles, with a spherical shape are also observed. These particles pile up to form a loose coating with a high porosity. Figure 8(b) indicates a coating microstructure consisting of splats and spherical particles. The spherical particles adhere to the surface of splats tightly to form a coating with few pores. Figure 8(c) shows a microstructure exhibiting well formed splats. Although some spherical particles can be seen, the microstructure consists mainly of splats and suggests that particles were well-melted in the plasma and form a dense coating with low porosity. Fig. 8(d) shows a microstructure consisting of over-molten splats. Cracks were formed in the coating due to thermal stress created in the spray process. It can be concluded from the SEM micrographs that the spray power level greatly effects the melting of hydroxyapatite powder, thus creating hydroxyapatite coatings with a variety of microstructures.

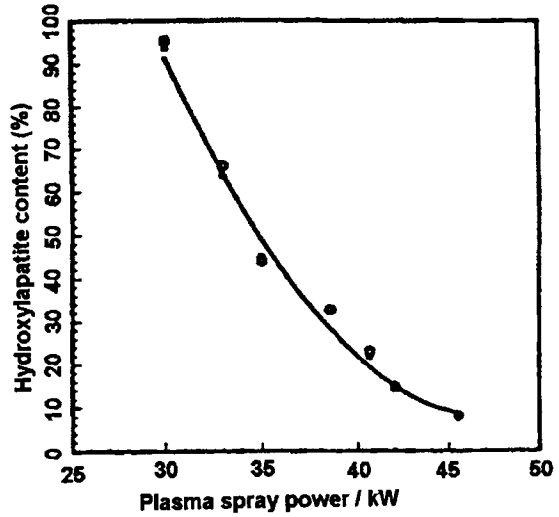

Fig. 5 Relationship between spray power and coating crystallinity

4. Conclusions

Amorphous phase formation and decomposition of hydroxyapatite occurs in VPS. Spray power level has an effect on characteristics of as-sprayed coatings. When the spray power changes from 30 kW to 45.5 kW, the crystallinity of as-sprayed coatings decreases significantly from 96-8%, indicating that the amorphous phase content of as-sprayed coatings depends greatly on the power level. Also, the Ca/P molar ratio of the coatings increased from 1.67 to 2.26, indicating that the decomposition of as-sprayed coatings is promoted by an increase in spray

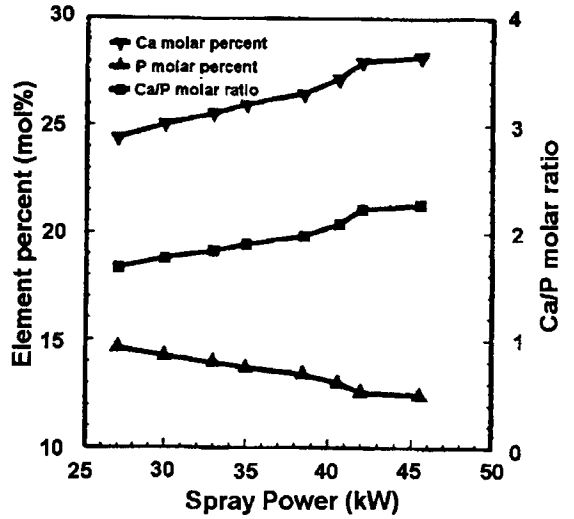

Fig. 6 Relationship between spray power levels and Ca/P molar ratio of as-sprayed hydroxyapatite coatings

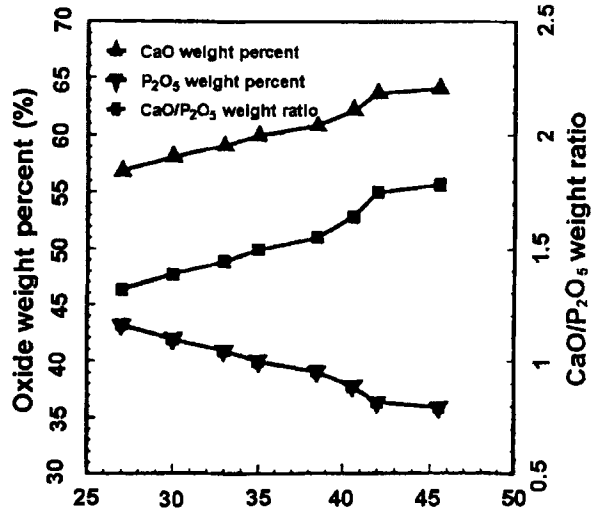

Fig. 7 Relationship between spray power levels and composition of as-sprayed hydroxyapatite coatings

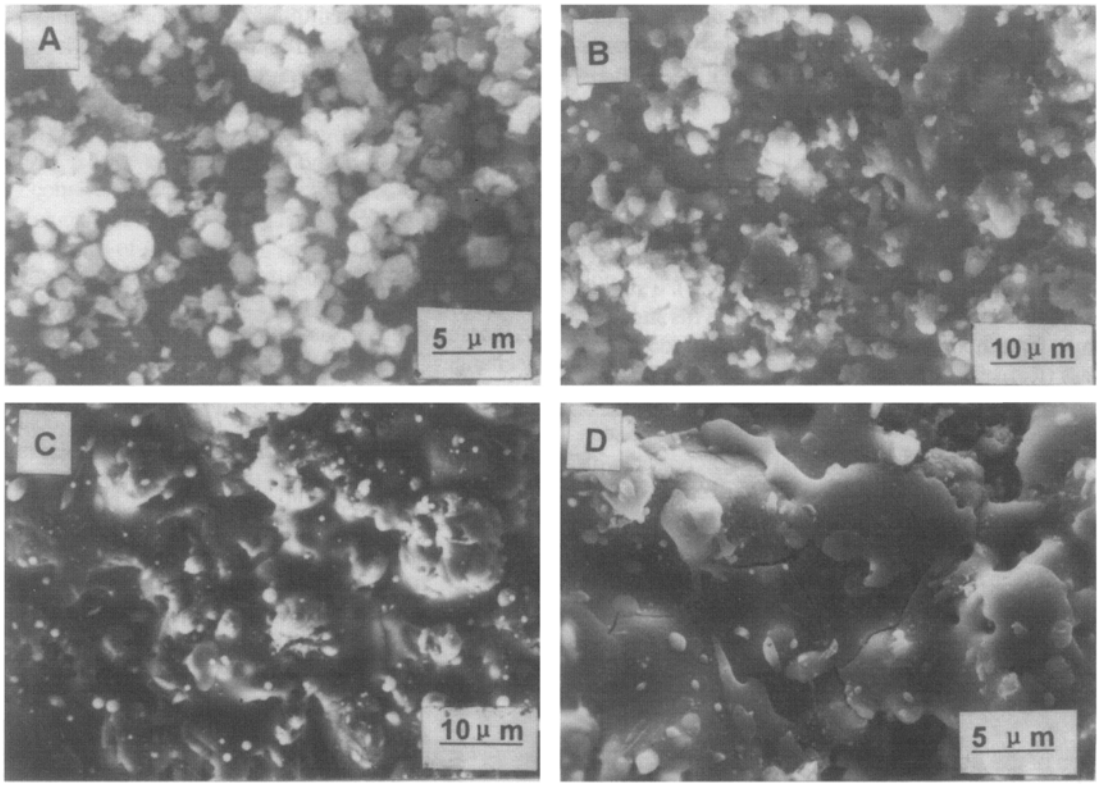

Fig. 8 Surface morphology of as-sprayed coatings. (a) HA coating sprayed at 30 kW. (b) HA coating sprayed at 35 kW. (c) HA coating sprayed at 40.6 kW. (d) HA coating sprayed at 45.5 kW

power level. SEM micrographs reveal that these effects can possibly be linked to the melting behavior of the starting powder. At different spray power levels, the starting powder experiences a process from unmelted to overmelted, creating coatings with a different microstructure.

References

1. S. Ozawa and S. Kasugai, Evaluation of Implant Materials (Hydroxyapatite, Glass-ceramics, Titanium) in Rat Bone Marrow Stromal Cell Culture, *Biomater.*, Vol 17, 1996, p 23-29
2. V. Passi, V. Tarrible, W. Marin, A. Miotti, and A. Pareti, Hydroxyapatite in Oral Surgery: Clinical and Histological Results, *Ceramics in Substitutive and Reconstructive Surgery*, P. Vincenzini, Ed., Elsevier, 1991, p 467-476
3. B.W. Schreurs, R. Huiskes, P. Buma, and T. J. H. Slooff, Biomedical and Histological Evaluation of a Hydroxyapatite-Coated Titanium Femoral Stem Fixed with an Intramedullary Morsellized Bone Grafting Technique: An Animal Experiment on Goat, *Biomater.*, Vol 17, 1996, p 1177-1186
4. J.A. Jansen, J.P.C.M. Van Der Waerden, and J.G.C. Wolke, A Histological Evaluation of the Effect of Hydroxyapatite Coating on Interfacial Response, *J. Mater. Sci.: Mater. Med.*, Vol 4, 1993, p 466-470
5. J. Li and L. Hermansoon, Mechanical Evaluation of Hot Isostatically Pressed Hydroxyapatite, *Interceram*, Vol 39 (No. 2), 1990, p 13-15
6. M. Akao, H. Aoki, and K. Kato, Mechanical Properties of Sintered Hydroxyapatite for Prosthetic Application, *J. Mater. Sci.*, Vol 16, 1981, p 809-812
7. M. Jarcho, C.H. Bolen, M.B. Thomas, J. Bobick, J.F. Kay, and R.H. Doremus, Hydroxyapatite Synthesis and Characterization in Dense Polycrystalline Form, *J. Mater. Sci.*, Vol 11, 1976, p 2027-2035
8. K.A. Gross and C.C. Berndt, Thermal Spraying of Hydroxyapatite for Bioceramic Applications, *Key Eng. Mater.*, Vol 53-55, 1991, p 124-129
9. M. Schirkhanzadeh, Bioactive Calcium Phosphate Coatings Prepared by Electrodeposition, *J. Mater. Sci. Lett.*, Vol 10, 1991, p 1415-1417
10. M. Schirkhanzadeh, Electrochemical Fabrication of Bioactive Composite Coatings on Ti6Al4V Surgical Alloy, *Mater. Lett.*, Vol 14, 1992, p 27-30
11. P. Li, K. de Groot, and T. Kokubo, Bioactive $Ca_{10}(PO_4)_6(OH)_2$-TiO_2 Composite Coating Prepared by Sol-Gel Process, *J. Sol-gel Sci. Technol.*, Vol 7, 1996, p 27-34
12. H. Oguchi and G.W. Hastings, In Vivo Evaluation of Hydroxyapatite Sprayed by Different Coating Methods-One Year After Implantation, *Bioceram.*, Vol 7, Ed., O.H. Andersson, 1994, p 215-221
13. K.A. Gross and C.C. Berndt, The Amorphous Phase in Plasma Sprayed Hydroxyapatite Coatings, *Bioceram.*, Vol 8, J. Wilson, L.L. Hench, and D. Greenspan, Ed., Pergaman Press, 1995, p 361-368
14. T. Weidong, C. Jiyong, and Z. Xingdong, Amorphorization and Recrystallization During Plasma Spraying of Hydroxyapatite, *Biomater.*, Vol 16, 1995, p 829-832
15. E. L. Ellies, Crystallographic Changes in Calcium Phosphates during Plasma Spraying, *Biomater.*, Vol 13 (No. 5), 1991, p 313-317
16. K.A. Gross and C.C. Berndt, Optimization of Spraying Parameters for Hydroxyapatite, 2nd Plasma Technik Symposium, Vol 3, S. Bum. Sondmeier, H. Eschnduer, P. Huber, and A.R. Nicoll, Ed., Plasma Technik AG, Lucerne, Switzerland, 1991, p 159-170